Featured in Physics

# Raman Probing the Local Ultrastrong Coupling of Vibrational Plasmon Polaritons on Metallic Gratings

Rakesh Arul,[1] Kishan Menghrajani,[2] Marie S. Rider,[2] Rohit Chikkaraddy,[1] William L. Barnes,[2,*] and Jeremy J. Baumberg[1,†]

[1]*NanoPhotonics Centre, Cavendish Laboratory, Department of Physics, JJ Thompson Avenue, University of Cambridge, Cambridge, CB3 0HE, United Kingdom*

[2]*Department of Physics and Astronomy, University of Exeter, Exeter, EX4 4QL, United Kingdom*

(Received 29 March 2023; accepted 12 July 2023; published 22 September 2023)

Strong coupling of molecular vibrations with light creates polariton states, enabling control over many optical and chemical properties. However, the near-field signatures of strong coupling are difficult to map as most cavities are closed systems. Surface-enhanced Raman microscopy of open metallic gratings under vibrational strong coupling enables the observation of spatial polariton localization in the grating near field, without the need for scanning probe microscopies. The lower polariton is localized at the grating slots, displays a strongly asymmetric line shape, and gives greater plasmon-vibration coupling strength than measured in the far field. Within these slots, the local field strength pushes the system into the ultrastrong coupling regime. Models of strong coupling which explicitly include the spatial distribution of emitters can account for these effects. Such gratings enable exploration of the rich physics of polaritons, its impact on polariton chemistry under flow conditions, and the interplay between near- and far-field properties through vibrational polariton-enhanced Raman scattering.

DOI: 10.1103/PhysRevLett.131.126902

The interaction of light with ensembles of resonant two-level systems within a cavity of sufficient finesse can reach the strong coupling regime [1]. This manifests as a Rabi splitting of the original resonance into upper and lower polariton modes, besides uncoupled "dark" states. Under strong coupling, many properties of the coupled emitter-photon system change, including chemical reactivities [2] and single photon nonlinearities [3]. Strong coupling has previously been achieved within single antenna-single emitter structures [4–6], high-finesse optical [3,7] and microwave resonators [8], and more recently in the midinfrared (IR) regime with vibrational strong coupling enabled by plasmonic metasurfaces [9–12]. The IR regime holds several advantages for strong coupling including large dipole oscillator strengths, easier cavity fabrication, but especially direct access to molecular vibrations relevant to material properties. Typically, the energy and momentum of polaritons is probed through far-field scattering and emission spectroscopies. However, the requirement for high-finesse cavities implies that little light escapes outside the cavity resonances, limiting optical interrogation of near-field variations in polariton modes, which is expected to show rich physics. Probing the near-field of systems under strong coupling, which previously required challenging scanning near-field optical microscopies [13], constitutes an open problem in understanding light-matter interactions on subwavelength scales [14].

Surface plasmon polaritons (SPPs) at a metal-dielectric interface lie outside the light line and cannot be excited by incident far-field radiation due to the momentum-mismatch. By structuring a metallic surface with a periodic grating, the optical wave vector acquires multiples of $k_g = 2\pi n_m/\Lambda$, for grating period $\Lambda$ and refractive index $n_m$ of the medium around the grating. At a metal-dielectric interface SPPs can thus be multiply scattered and form Bloch waves. Far-field radiation may then couple to the plasmonic grating modes, and in the near field can couple to molecular transitions ($\omega_0$) such as vibrational IR absorptions.

When an IR-active vibration is simultaneously Raman active, polariton modes are also expected to appear in the Raman spectra in the ultrastrong coupling regime [15–17] [Fig. 1(c)]. Despite such predictions, dark modes dominate the Raman scattering, preventing conclusive demonstrations of vibropolaritonic Raman in microcavities [18–20] or open metasurfaces [12,21], although Raman scattering can be seen for phonon polaritons in the Restrahlen bands of bulk crystals [22,23]. Here, we show that surface-enhanced Raman (SERS) microscopy of micron-scale open gratings experiencing infrared vibrational strong coupling, which we term polariton-enhanced Raman spectroscopy (VibPERS),

*Published by the American Physical Society under the terms of the Creative Commons Attribution 4.0 International license. Further distribution of this work must maintain attribution to the author(s) and the published article's title, journal citation, and DOI.*

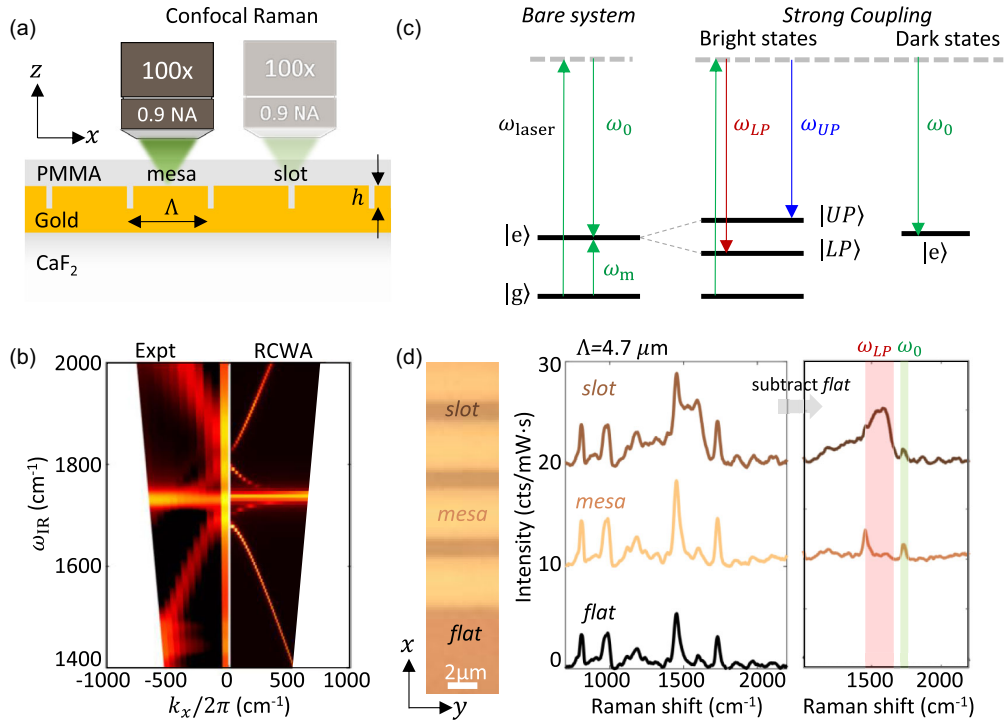


FIG. 1. Strong coupling in open gratings. (a) Raman microscopy (pump 532 nm) of grating (period $\Lambda = 4.7$ μm, slot width 1 μm, height $h = 0.1$ μm, with 1 μm thick PMMA layer). (b) Grating IR reflectance spectra in experiment (expt, left) and theory (RCWA, right). (c) Raman scattering from ground state $|g\rangle$ to excited state $|e\rangle$ or VibPERS to lower $|\mathrm{LP}\rangle$ and upper $|\mathrm{UP}\rangle$ polariton states. (d) VibPERS spectra of slot and mesa in grating compared to flat regions. Left: Optical image of grating. Middle: Background-corrected Raman spectra. Right: Raman spectra of slot and mesa after subtracting flat spectrum.

enables us to detect the localization and energy of polaritons in the near field of the grating. This also eliminates the need for perturbing tip-based scanning probe microscopies.

VibPERS spectra of gratings under vibrational strong coupling are measured using a confocal Raman microscope [Fig. 1(a)] with a tightly focused (100× objective, 0.9 NA) 532 nm excitation laser (see Supplemental Material [24], Methods). The IR transmission spectra of the gratings display a clear anticrossing of the polariton modes at normal incidence, when the $\Lambda = 4.7$ μm grating mode strongly couples with the C = O stretch of PMMA ($\omega_0 = 1732$ cm$^{-1}$) at normal incidence [Fig. 1(b)]. This matches a rigorous coupled wave analysis (RCWA [25]) model [Fig. 1(b)]. Fitting the Hopfield model yields a Rabi splitting $\Omega_{\mathrm{Rabi}} = 95$ cm$^{-1}$, which exceeds the linewidths of the original plasmonic grating mode (45 cm$^{-1}$) and absorption at $\omega_0$ (Supplemental Material [24], Sec. S2).

Open gratings allow Raman spectral mapping as a function of lateral position and height. This reveals three distinct Raman signatures: from the flat (reference) region, from the middle of the grating mesa, and from the grating slot [Fig. 1(d)]. The flat region shows expected PMMA peaks, which are enhanced on the gold-coated mesa due to increased reflectivity from the gold. In the slots however, there is a clear extra contribution in the 1000–1600 cm$^{-1}$ region. Removing the background contribution reveals the spectral signature of this extra contribution [Fig. 1(d) right, brown], which is attributed to the lower polariton $|\mathrm{LP}\rangle$ state [see Fig. 1(c)]. The extracted $|\mathrm{LP}\rangle$ spectrum is localized within the slot and displays an asymmetric shape peaked at ~1600 cm$^{-1}$ ($\omega_{\mathrm{LP}}$). The possibility of molecular damage, as observed elsewhere [18,19], is discounted through intensity-dependent measurements that reveal different peaks associated with molecular damage while the original PMMA peaks remain unchanged (Supplemental Material [24], Sec. S4). No signal from the upper polariton mode $|\mathrm{UP}\rangle$ is observed, however. A broad electronic Raman scattering (ERS) or photoluminescence background is also present in the slot VibPERS spectra (Supplemental Material [24], Fig. S3c) due to excitation of edge plasmon modes.

*Spatial Raman mapping of LP.*—The observed $|\mathrm{LP}\rangle$ signature is enhanced and localized in the slot region of the $\Lambda = 4.7$ μm grating, while the PMMA molecular band $\omega_0$ is only weakly enhanced [Figs. 2(b), 2(c), 2(d), and Supplemental Material [24], Sec. S3]. The $|\mathrm{LP}\rangle$ signature is seen to be localized within the slots when focussing $z = 1$ μm above the grating surface and resolved to be at the slot edges when focussing exactly on the surface ($z = 0$ μm). This is more clearly visible in the laterally averaged plots [Figs. 2(e), 2(g)]. The extracted energy separation between the peak of the $|\mathrm{LP}\rangle$ and $\omega_0$ at each location in the slots reveals an average near-field coupling strength $g$ of

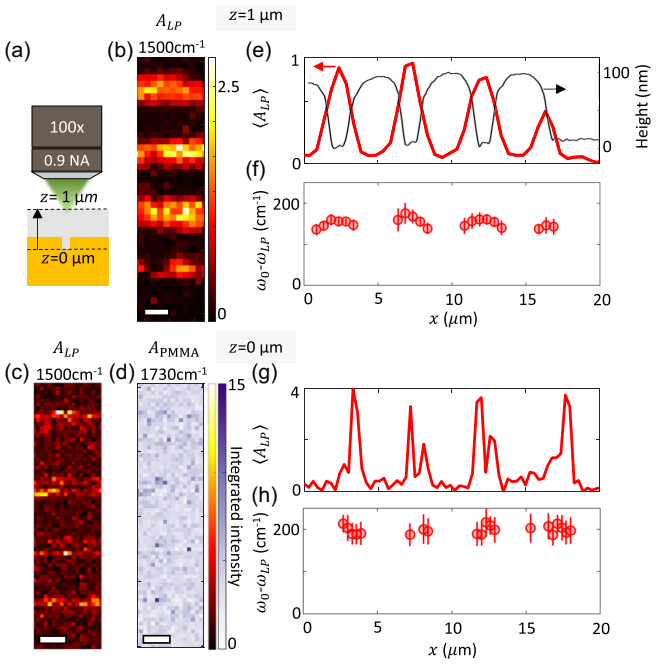


FIG. 2. Lower polariton enhanced Raman and localization in grating slots. (a) Raman maps acquired at two different heights above the grating surface. (b) Raman map at PMMA surface ($z = 1$ μm) showing integrated peak area of lower polariton ($A_{\mathrm{LP}}$). (c, d) Raman maps at grating surface ($z = 0$ μm) for (c) LP ($A_{\mathrm{LP}}$) and (d) PMMA ($A_{\mathrm{PMMA}}$) modes with shared spectrally integrated intensity scale. White scale bars are 2 μm. (e)–(h) Laterally averaged $A_{\mathrm{LP}}$ and $\omega_{\mathrm{LP}}$-$\omega_0$ across the grating for (e),(f) $z = 1$ and (g),(h) $z = 0$ μm.

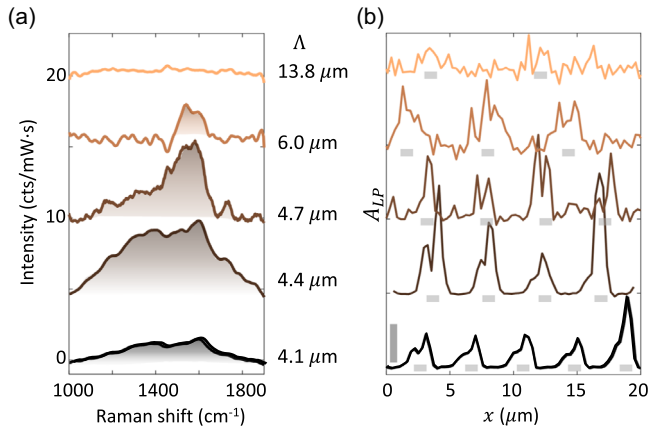


FIG. 3. Detuning of grating modes. (a) VibPERS spectra of lower polariton mode for different grating periods (Λ). (b) Laterally averaged lower polariton mode (integrated area) *vs* $x$ position, which is localized at the grating slots (vertical bar is 100 cts · cm$^{-1}$ mW$^{-1}$ s$^{-1}$). Horizontal gray bars indicate slot positions.

$174 \pm 30$ cm$^{-1}$, much larger than measured in the far field through IR transmission (47.5 cm$^{-1}$).

To further confirm this assignment of $|\mathrm{LP}\rangle$ polariton-enhanced Raman scattering (VibPERS), the dependence on grating mode detuning from $\omega_0$ is examined (Fig. 3). Changing the periodicity of the grating from 4 to 14 μm shifts this detuning (Supplemental Material [24], Sec. S5), as the position of the anticrossing moves to higher wave vector, away from normal incidence (Supplemental Material [24], Fig. S10). This manifests as a reduced spectral weight and asymmetry in the $|\mathrm{LP}\rangle$ VibPERS spectrum for $\Lambda = 6$ μm [Fig. 3(a)]. For $\Lambda = 13.8$ μm, it is the second-order grating mode which now couples to $\omega_0$, however, no clear VibPERS signal is observed, perhaps due to the greater sensitivity of the higher-order mode to fabrication imperfections. Only for anticrossings at near normal incidence is the strong $|\mathrm{LP}\rangle$ VibPERS seen. Averaging the spectral area of the $|\mathrm{LP}\rangle$ mode while scanning across the grating [Fig. 3(b)] confirms that it is always localized at the slots. The dependence of the intensity of $|\mathrm{LP}\rangle$ VibPERS signals can be attributed to the different local field enhancements of the Raman excitation laser within the slots depending on the grating period (Supplemental Material [24], Sec. S6).

*Understanding localized polariton Raman scattering.*— To explain the localization of the $|\mathrm{LP}\rangle$ signal within the slots, the $|\mathrm{LP}\rangle$ asymmetric VibPERS spectrum, the lack of an upper polariton signal, and the larger near-field Rabi splitting, we perform near-field electromagnetic simulations and develop a simplified theory for Raman scattering of polaritons within gratings. The $|\mathrm{LP}\rangle$ VibPERS intensity depends on the localization of the infrared polariton (~1681 cm$^{-1}$) and the visible Raman pump (532 nm). Finite-difference time-domain (FDTD) simulations show the $|\mathrm{LP}\rangle$ optical near-field ($E_x$) is indeed tightly localized at the slot edges on the grating surface at $z = 0$ μm [Fig. 4(a)]. The 532 nm laser field is uniformly enhanced on the facet and at the slot edges (Supplemental Material [24], Fig. S14c). Hence, their combined impact is to out-couple the $|\mathrm{LP}\rangle$ VibPERS signals more effectively from the slot edges.

The asymmetry of the $|\mathrm{LP}\rangle$ VibPERS signal is likely due to angle averaging inherent in confocal Raman microscopy with a high numerical-aperture objective to get spatial profiles [27] (further discussed in Supplemental Material [24], Sec. S9). The visible-frequency Raman dipoles sample the $|\mathrm{LP}\rangle$ across a range of momentum $k_x$ in the infrared [Fig. 1(b)], which broadens the range of frequencies measured. The fraction of molecular oscillator in each hybrid polariton state changes with momentum $k_x$, and is quantified by the Hopfield coefficient $b_{\mathrm{LP,UP}}$ as a function of angle for the $|\mathrm{LP}\rangle$ and $|\mathrm{UP}\rangle$ [Fig. 4(b)]. The molecular fraction contributes to VibPERS, so using density-of-states estimates [18], we weight each simulated reflectance spectrum (Supplemental Material [24], Sec. S3) with its molecular fraction and evaluate the sum up to the numerical aperture of our objective lens. The resulting spectrum is asymmetric [Fig. 4(c)] with a significant low-frequency tail as observed in experiments [Fig. 1(d)]. We note this

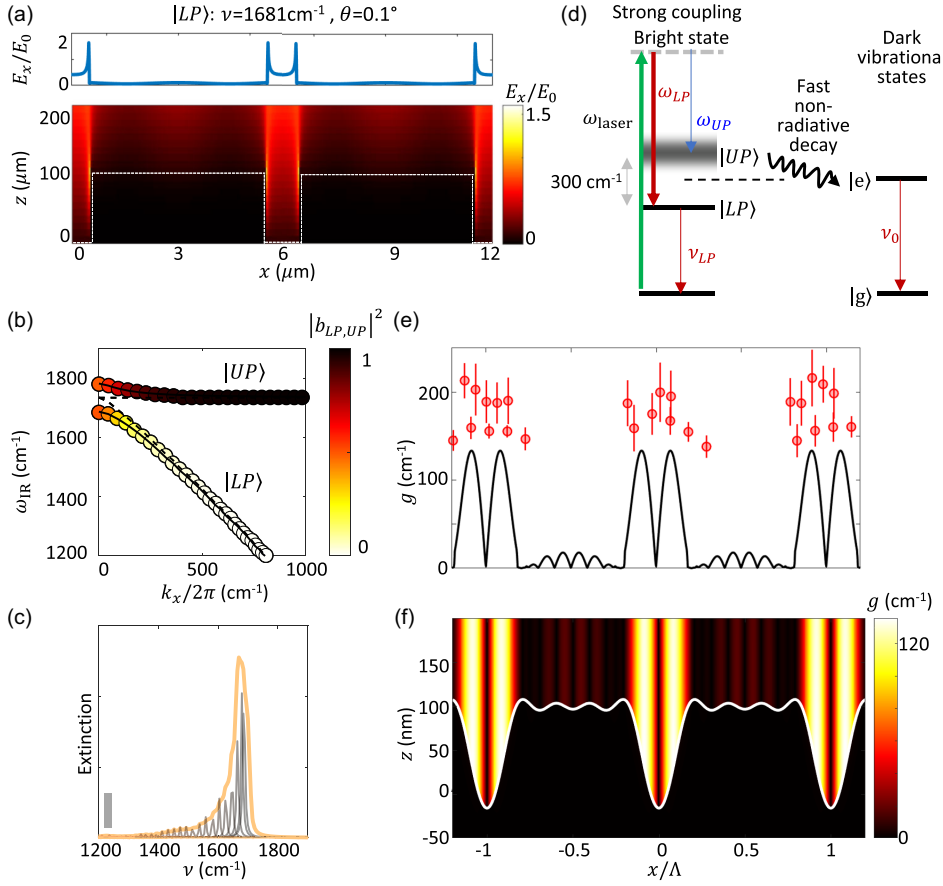


FIG. 4. Polariton-enhanced Raman scattering in gratings. (a) Field distribution ($E_x/E_0$) for the lower polariton under near-normal incidence ($\theta = 0.1°$) transverse-magnetic (TM) excitation perpendicular to the grating grooves (dashed). Gold permittivity from Ref. [26]. (b) Coupled oscillator fit to RCWA simulations of grating scattering for upper and lower polariton modes *vs* momentum ($k_x$). Colors show vibrational Hopfield coefficient fraction (Supplemental Material, Sec. S2 [24]). (c) Molecular density-of-states (corrected and angle-averaged) showing asymmetric broadening of LP peak (gray bar indicating extinction of 0.1). (d) Polariton states showing scattering from ground state to bright (strongly coupled) and dark states, labeling Raman scattering ($\omega$) and infrared absorption ($\nu$). (e) Plasmon-vibration coupling strength $g$ vs normalized position $x/\Lambda$, with red points from Fig. 2. (f) Map of spatial plasmon-vibration coupling strength $g$ along the $\Lambda = 4.7$ μm grating (modeled surface profile in white).

approximation only considers the $k_x$ momentum component and not the full parabolic dispersion including $k_y$. By contrast, the $|\mathrm{UP}\rangle$ VibPERS signal is suppressed due to fast nonradiative decay of the upper polaritons into the reservoir of dark vibrational states present in the system, and the lower molecular fraction of $|\mathrm{UP}\rangle$ states at small $k_x$ [Fig. 4(b)]. This is analogous to electronic strong coupling, where only emission from the lower polariton branch is detected at room temperature [28].

Finally, the experimentally observed enhanced near-field Rabi splitting (distinct from far field) is recovered in our theoretical model showing spatial variation in molecule-plasmon coupling constant $g$ due to spatial variation in the optical field strength. The dominant contribution to the lower and upper polariton optical fields comes from the coupled first-order ($\pm 2\pi/\Lambda$) grating-scattered branches of the surface plasmon [29,30]. Using the Chandezon method [31] to calculate the contribution to the optical field from the lower grating-scattered branch at $k_x = 0$ from a rectangular grating (Supplemental Material [24], Sec. S7), we find the spatially dependent light-molecule coupling from $g_i(x,z) \approx -\mu_i \cdot \boldsymbol{E}(x,z)$, where $g_i$ is the plasmon-vibration coupling strength for molecule $i$ in position $x$ on the grating at height $z$ from the gold surface, $\boldsymbol{E}$ is the optical field associated with the lower grating-scattered branch at $k_x = 0$, and $\mu_i$ is the vibration IR transition dipole moment. While the effective coupling strength [32] $\langle g \rangle = \sqrt{\sum_i g_i^2}$ is measured in far-field extinction spectra, in the near-field molecules experience a spatially varying $g_{\mathrm{NF}}$ which is maximum near slot edges and greatly reduced on the mesa [Figs. 4(e)–4(f)], directly seen in the VibPERS spectra of the $|\mathrm{LP}\rangle$ state, and can greatly exceed the far-field mean $\langle g \rangle$. The value of $g_{\mathrm{NF}}$ has an upper bound given by the bulk optical parameters of PMMA [33]. We find that this maximum value ~140 cm$^{-1}$ (Supplemental Material [24], Sec. S8) is consistent with the maximum near-field value

we find here of $174 \pm 30\ \mathrm{cm}^{-1}$. Thus, any near-field enhancement of the strong coupling effect can at most place the LP at $\sim 1590\ \mathrm{cm}^{-1}$, broadly consistent with our observations. We note that this bulk limit may help resolve the thus-far puzzling observations of Shalabney *et al.* [20,34] and Menghrajani *et al.* [9], both of whom found Raman features at $\sim 1590\ \mathrm{cm}^{-1}$; both might be due to Raman signals associated with localized modes. This highlights the role of (i) the visible wavelength SERS effect in amplifying signals from a small number of molecules at edges, and (ii) localized hot spots in the infrared that couple to the dispersive grating mode giving rise to the large coupling strength $g$ measured in VibPERS. The large near-field $g_{\mathrm{NF}} = 174 \pm 30\ \mathrm{cm}^{-1}$ pushes the system into the ultrastrong coupling regime ($\omega_{\mathrm{Rabi}}/\omega_0 = 0.2 > 0.1$), with clear effects on Raman spectra as predicted [16,17].

Visible Raman scattering from polaritons in the infrared enables sub-IR-wavelength visualization of vibropolaritons in open grating systems under strong coupling. Tightly focused visible laser excitation fulfils the scattering momentum conservation for polariton modes out to the light-line, resulting in an asymmetric lineshape due to angle-weighted contributions to lower polariton mode Raman signals. Raman maps probe the local density-of-polaritonic-states and show signatures of ultrastrong coupling ($\omega_{\mathrm{Rabi}}/\omega_0 \sim 0.2$) in the near field despite only being in strong coupling in the far-field. A small mode volume in the IR is critical to observe splitting effects in polariton-enhanced Raman scattering—previous measurements in microcavities and plasmonic surface lattice resonators [9–11] probed much larger mode volumes $\geq \lambda^3$. The ultrastrong coupling regime [35] results in virtual photons in the ground state, potentially changes the material physicochemical properties, and can induce photon blockade [36], nonclassical state generation [37], and superradiant phase transitions [38]. This system forms a platform for discoveries in infrared or THz interactions with molecular vibrational oscillators.

Research data are available in [39].

We acknowledge useful discussions with Rubén Esteban, Unai Muniain, and Javier Aizpurua. We acknowledge support from European Research Council (ERC) under Horizon 2020 research and innovation programme THOR (Grant Agreement No. 829067), PICOFORCE (Grant Agreement No. 883703), and project PHOTMAT (Grant Agreement ERC-2016-AdG-742222). R. A. acknowledges support from the Rutherford Foundation of the Royal Society Te Apārangi of New Zealand, and the Winton Programme for the Physics of Sustainability. R. C. and R. A. acknowledge support from Trinity College, University of Cambridge. K. S. M. acknowledges financial support from the Leverhulme Trust research grant "Synthetic biological control of quantum optics".

*Corresponding author: W.L.Barnes@exeter.ac.uk
†Corresponding author: jjb12@cam.ac.uk

[1] A. F. Kockum, A. Miranowicz, S. De Liberato, S. Savasta, and F. Nori, Ultrastrong coupling between light and matter, Nat. Rev. Phys. **1**, 19 (2019).
[2] F. J. Garcia-Vidal, C. Ciuti, and T. W. Ebbesen, Manipulating matter by strong coupling to vacuum fields, Science **373**, 0336 (2021).
[3] A. Pscherer, M. Meierhofer, D. Wang, H. Kelkar, D. Martín-Cano, T. Utikal, S. Götzinger, and V. Sandoghdar, Single-Molecule Vacuum Rabi Splitting: Four-Wave Mixing and Optical Switching at the Single-Photon Level, Phys. Rev. Lett. **127**, 133603 (2021).
[4] R. Chikkaraddy, B. De Nijs, F. Benz, S. J. Barrow, O. A. Scherman, E. Rosta, A. Demetriadou, P. Fox, O. Hess, and J. J. Baumberg, Single-molecule strong coupling at room temperature in plasmonic nanocavities, Nature (London) **535**, 127 (2016).
[5] J. P. Reithmaier, G. Sęk, A. Löffler, C. Hofmann, S. Kuhn, S. Reitzenstein, L. Keldysh, V. Kulakovskii, T. Reinecke, and A. Forchel, Strong coupling in a single quantum dot–semiconductor microcavity system, Nature (London) **432**, 197 (2004).
[6] O. Bitton and G. Haran, Plasmonic cavities and individual quantum emitters in the strong coupling limit, Acc. Chem. Res. **55**, 1659 (2022).
[7] T. Aoki, B. Dayan, E. Wilcut, W. P. Bowen, A. S. Parkins, T. Kippenberg, K. Vahala, and H. Kimble, Observation of strong coupling between one atom and a monolithic microresonator, Nature (London) **443**, 671 (2006).
[8] G. Rempe, H. Walther, and N. Klein, Observation of Quantum Collapse and Revival in a One-Atom Maser, Phys. Rev. Lett. **58**, 353 (1987).
[9] K. S. Menghrajani, G. R. Nash, and W. L. Barnes, Vibrational strong coupling with surface plasmons and the presence of surface plasmon stop bands, ACS Photonics **6**, 2110 (2019).
[10] Z. T. Brawley, S. D. Storm, D. A. Contreras Mora, M. Pelton, and M. Sheldon, Angle-independent plasmonic substrates for multi-mode vibrational strong coupling with molecular thin films, J. Chem. Phys. **154**, 104305 (2021).
[11] B. Cohn, K. Das, A. Basu, and L. Chuntonov, Infrared open cavities for strong vibrational coupling, J. Phys. Chem. Lett. **12**, 7060 (2021).
[12] F. Verdelli, J. J. Schulpen, A. Baldi, and J. G. Rivas, Chasing vibro-polariton fingerprints in infrared and raman spectra using surface lattice resonances on extended metasurfaces, J. Phys. Chem. C **126**, 7143 (2022).
[13] A. Bylinkin, M. Schnell, F. Calavalle, P. Li, J. Taboada-Gutièrrez, S. Liu, J. H. Edgar, F. Casanova, L. E. Hueso, and P. Alonso-Gonzalez, Real-space observation of vibrational strong coupling between propagating phonon polaritons and organic molecules, Nat. Photonics **15**, 197 (2021).
[14] W. M. Takele, F. Wackenhut, L. Piatkowski, A. J. Meixner, and J. Waluk, Multimode vibrational strong coupling of methyl salicylate to a Fabry-Pérot microcavity, J. Phys. Chem. B **124**, 5709 (2020).
[15] M. A. Zeb, P. G. Kirton, and J. Keeling, Exact states and spectra of vibrationally dressed polaritons, ACS Photonics **5**, 249 (2018).

[16] J. del Pino, J. Feist, and F. Garcia-Vidal, Signatures of vibrational strong coupling in Raman scattering, J. Phys. Chem. C **119**, 29132 (2015).
[17] A. Strashko and J. Keeling, Raman scattering with strongly coupled vibron-polaritons, Phys. Rev. A **94**, 023843 (2016).
[18] W. Ahn and B. Simpkins, Raman scattering under strong vibration-cavity coupling, J. Phys. Chem. C **125**, 830 (2020).
[19] W. M. Takele, L. Piatkowski, F. Wackenhut, S. Gawinkowski, A. J. Meixner, and J. Waluk, Scouting for strong light–matter coupling signatures in Raman spectra, Phys. Chem. Chem. Phys. **23**, 16837 (2021).
[20] A. Shalabney, J. George, H. Hiura, J. A. Hutchison, C. Genet, P. Hellwig, and T. W. Ebbesen, Enhanced raman scattering from vibro-polariton hybrid states, Angew. Chem., Int. Ed. **54**, 7971 (2015).
[21] K. S. Menghrajani, M. Chen, K. Dholakia, and W. L. Barnes, Probing vibrational strong coupling of molecules with wavelength-modulated Raman spectroscopy, Adv. Opt. Mater. **10**, 2102065 (2022).
[22] C. Henry and J. Hopfield, Raman Scattering by Polaritons, Phys. Rev. Lett. **15**, 964 (1965).
[23] Y. N. Polivanov, Raman scattering of light by polaritons, Sov. Phys. Usp. **21**, 805 (1978).
[24] See Supplemental Material at http://link.aps.org/supplemental/10.1103/PhysRevLett.131.126902 for experimental methods, electromagnetic simulations, theoretical model details of the Chandezon method, power- and acquisition time-dependent Raman spectra to exclude molecular damage, and depth mapping of Raman spectra.
[25] J.-M. Manceau, S. Zanotto, I. Sagnes, G. Beaudoin, and R. Colombelli, Optical critical coupling into highly confining metal-insulator-metal resonators, Appl. Phys. Lett. **103**, 091110 (2013).
[26] D. R. Lide, *CRC Handbook of Chemistry and Physics* (CRC Press, Boca Raton, 2004), Vol. 85.
[27] Z. Geng, J. Theenhaus, B. K. Patra, J.-Y. Zheng, J. Busink, E. C. Garnett, and S. R. Rodriguez, Fano lineshapes and Rabi splittings: Can they be artificially generated or obscured by the numerical aperture?, ACS Photonics **8**, 1271 (2021).
[28] D. Lidzey, D. Bradley, T. Virgili, A. Armitage, M. Skolnick, and S. Walker, Room Temperature Polariton Emission from Strongly Coupled Organic Semiconductor Microcavities, Phys. Rev. Lett. **82**, 3316 (1999).
[29] M. S. Rider, R. Arul, J. J. Baumberg, and W. L. Barnes, Theory of strong coupling between molecules and surface plasmons on a grating, Nanophotonics **11**, 3695 (2022).
[30] W. L. Barnes, T. Preist, S. Kitson, and J. Sambles, Physical origin of photonic energy gaps in the propagation of surface plasmons on gratings, Phys. Rev. B **54**, 6227 (1996).
[31] J. Chandezon, G. Raoult, and D. Maystre, A new theoretical method for diffraction gratings and its numerical application, J. Opt. **11**, 235 (1980).
[32] A. González-Tudela, P. Huidobro, L. Martín-Moreno, C. Tejedor, and F. García-Vidal, Theory of Strong Coupling Between Quantum Emitters and Propagating Surface Plasmons, Phys. Rev. Lett. **110**, 126801 (2013).
[33] M. Barra-Burillo, U. Muniain, S. Catalano, M. Autore, F. Casanova, L. E. Hueso, J. Aizpurua, R. Esteban, and R. Hillenbrand, Microcavity phonon polaritons from the weak to the ultrastrong phonon–photon coupling regime, Nat. Commun. **12**, 6206 (2021).
[34] A. Shalabney, J. George, J. a. Hutchison, G. Pupillo, C. Genet, and T. W. Ebbesen, Coherent coupling of molecular resonators with a microcavity mode, Nat. Commun. **6**, 5981 (2015).
[35] P. Forn-Díaz, L. Lamata, E. Rico, J. Kono, and E. Solano, Ultrastrong coupling regimes of light-matter interaction, Rev. Mod. Phys. **91**, 025005 (2019).
[36] A. Ridolfo, M. Leib, S. Savasta, and M. J. Hartmann, Photon Blockade in the Ultrastrong Coupling Regime, Phys. Rev. Lett. **109**, 193602 (2012).
[37] S. Ashhab and F. Nori, Qubit-oscillator systems in the ultrastrong-coupling regime and their potential for preparing nonclassical states, Phys. Rev. A **81**, 042311 (2010).
[38] K. C. Stitely, S. J. Masson, A. Giraldo, B. Krauskopf, and S. Parkins, Superradiant switching, quantum hysteresis, and oscillations in a generalized Dicke model, Phys. Rev. A **102**, 063702 (2020).
[39] 10.17863/CAM.100101.